JOURNAL OF THE AMERICAN CHEMICAL SOCIETY
Article
pubs.acs.org/JACS

# Tailoring Bimetallic Alloy Surface Properties by Kinetic Control of Self-Diffusion Processes at the Nanoscale

Michele Rizzi,[†,‡] Sara Furlan,[†,◆] Maria Peressi,[†,§] Alfonso Baldereschi,[†,‡,∥] Carlo Dri,[⊥,#] Angelo Peronio,[⊥,#] Cristina Africh,[#] Paolo Lacovig,[∇] Erik Vesselli,*[,⊥,#] and Giovanni Comelli[⊥,#]

[†]Physics Department, University of Trieste, Strada Costiera 11, I-34151 Trieste, Italy
[‡]Institute of Theoretical Physics, École Polytechnique Fédérale de Lausanne (EPFL), CH-1015 Lausanne, Switzerland
[§]IOM-CNR DEMOCRITOS, Theory@Elettra Group, Trieste, Italy and Italian Consortium on Materials Science and Technology (INSTM)
[∥]IOM-CNR DEMOCRITOS, Trieste, Italy
[⊥]Physics Department and CENMAT, University of Trieste, via Valerio 2, I-34127 Trieste, Italy
[#]IOM-CNR Laboratorio TASC, Area Science Park, S.S. 14 km 163.5, I-34149 Basovizza (Trieste), Italy
[∇]Sincrotrone Trieste S.C.p.A., Area Science Park, S.S. 14 km 163.5, I-34149 Trieste, Italy

Ⓢ *Supporting Information*

**ABSTRACT:** Achieving control of the nanoscale structure of binary alloys is of paramount importance for the design of novel materials with specific properties, leading to, for example, improved reaction rates and selectivity in catalysis, tailored magnetic behavior in electronics, and controlled growth of nanostructured materials such as graphene. By means of a combined experimental and theoretical approach, we show that the complex self-diffusion mechanisms determining these key properties can be mostly defined by kinetic rather than energetic effects. We explain how in the Ni−Cu system nanoscale control of self-diffusion and segregation processes close to the surface can be achieved by finely tuning the relative concentration of the alloy constituents. This allows tailoring the material functionality and provides a clear explanation of previously observed effects involved, for example, in the growth of graphene films and in the catalytic reduction of carbon dioxide.

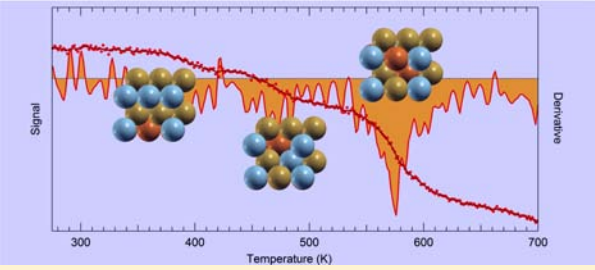

## INTRODUCTION

Binary alloys and their surfaces, interfaces, and junctions are intensively employed in the design of new technological nanodevices and nanostructured materials, with a large impact in many technological fields. Biocompatible materials, coatings, and electronic and magnetic devices are just a few examples among a large ensemble of possible applications that exploit the unique geometric, electronic, magnetic, chemical, mass transport, and segregation properties of binary alloys.[1] Specific examples are the use of nickel−aluminum alloys for nanoelectronics or protective coating purposes,[2−4] platinum−rhodium bimetallic compounds for their peculiar electrocatalytic properties,[5,6] and titanium-based alloys for mechanical and biological applications.[7,8] Another remarkable case is the recently observed ability of Ni−Cu to catalyze graphene growth from segregated carbon,[9] where precise control of the graphene layer morphology and growth process was achieved by fine-tuning the percentage of Ni atoms in the alloy. The effect is linked to the synergetic combination of the different carbon solubility in the two metals, together with the interplay between competing segregation effects.[10] Additionally, the graphene/Ni−Cu system shows peculiar oxidation resistance that has recently been investigated.[11] Ni−Cu alloys and ultrathin Ni films deposited on Cu substrates also exhibit magnetic properties that can be tailored by controlling the thickness of the Ni film and by properly selecting the crystallographic termination of the underlying Cu substrate.[12] Ni−Cu systems may additionally play a role in the catalytic synthesis of valuable fuels, for example, methanol or methane, obtained by selective reduction of carbon dioxide.[13−19] In the case of methanol synthesis, indirect control of Ni segregation at the Cu surface at high temperature is achieved by governing CO adsorption.[20−22]

Due to the above motivations, the Ni−Cu diffusion and segregation processes have been extensively investigated. However, despite all the devoted efforts, a thorough comprehension of the interplay between segregation, diffusion, and aggregation is still lacking. Little information is available concerning the small differences in the energy barriers defining many possible, competing mechanisms, and the role of kinetics is expected to be relevant. Fundamental studies in the literature report intermediate or "static" measurements with little

**Received:** July 31, 2012
**Published:** September 18, 2012

dynamic or kinetic experimental information. In a recent significant contribution,[23] the structure and the energetics of the buried Ni/Cu(001) interface are investigated and the energy differences between different Ni−Cu exchange configurations, as well as the strain relaxations, are found to be rather small, yielding single-atom energy differences of only a few tens of millielectronvolts between different geometric configurations, separated by energy barriers that can be overcome already at, or slightly above, room temperature when Ni−Cu exchange occurs close to the surface. It was therefore tentatively proposed that the atomic-scale structure of the Ni/Cu interface under reaction conditions is determined by kinetics rather than by energetics.[23] Providing a clear assessment of this open point represents the main drive of the present work. We prove that the nanoscale alloy structure is indeed determined by kinetics, which in turn, is mainly driven by the Ni concentration, providing a simple explanation to the observed tailoring capabilities of the alloy properties.

Concerning the evolution of Ni concentration on single crystal Cu terminations under ultrahigh vacuum (UHV) conditions,[21,22,24−27] it is already known that the growth of a Ni ad-layer with no intermixing requires Ni evaporation at low substrate temperatures (140−170 K) due to the low barrier for atomic Ni penetration into the Cu subsurface layers. A first annealing to intermediate temperatures (up to 300 K) yields Ni adatom diffusion and coalescence into two-dimensional (2D) Ni ad-islands in the submonolayer regime, while alloying at the Ni/Cu interface takes place at higher Ni coverage. Both surface alloying (i.e., in the first layer) and Ni diffusion into the Cu bulk occur for higher temperatures. The experimental information about the Ni depth profile is generally obtained ex situ or by means of indirect techniques such as temperature programmed desorption (TPD) of CO and $H_2$ used as probes,[21,22] or high-resolution electron energy loss spectroscopy (HREELS) of adsorbed CO,[24] which exhibits different coordination at adatom (ontop) and ad-dimer (bridge) Ni sites. However, the strong interaction of adsorbed molecular probes, such as CO, with Ni cannot be neglected, since it influences the segregation process itself, thus limiting the validity of the conclusions drawn from the observed behavior.

## ■ METHODS

**Experimental Section.** The Cu(110) sample was cleaned under UHV conditions by standard sputtering and annealing recipes. Ni was evaporated at a substrate temperature of 170 K from a pure, resistively heated Ni filament. A subsequent annealing of the surface up to 270 K yielded a good (1 × 1) ad-layer ordering without inducing Ni−Cu mixing for a Ni coverage lower than 2 ML. The deposition rate was calibrated by means of a quartz balance and a flux of 0.5 ML/min was adopted. Low energy electron diffraction (LEED) measurements were performed in a multipurpose UHV setup with a base pressure of $5 \times 10^{-11}$ mbar. Core-level photoelectron spectroscopy experiments were performed at the SuperESCA beamline of Elettra, the third-generation synchrotron radiation source in Trieste (Italy). Ni and Cu 3p core levels were measured at normal emission using 200 eV photons. A Phoibos hemispherical electron energy analyzer was used to collect the spectra with a time resolution of about 10 s in the time-resolved experiments. Binding energies were calibrated with respect to the Fermi level. After subtraction of a linear background, spectra were analyzed using a Doniach−Šunjić function,[28] convoluted with a Gaussian envelope in order to account for experimental resolution, inhomogeneity, and temperature-induced broadening. C and O 1s spectral regions were always checked in order to ensure sample cleanliness both prior and after Ni evaporation.

**First-Principles Calculations.** Calculation of equilibrium geometries, barriers, energies, and diffusion/segregation paths were performed within the framework of density functional theory (DFT) in the spin-polarized generalized gradient approximation using the Perdew−Burke−Ernzerhof exchange-correlation functional.[29] We used the plane-wave-based PWSCF codes of the QUANTUM-ESPRESSO (QE) distribution,[30] with publicly available ultrasoft pseudopotentials.[31] Slab geometries with a five-layer Cu slab plus a vacuum space of about 15 Å, that is, three times the slab thickness, were used to simulate the Ni−Cu surface. On the basis of a comparison of structural parameters and electronic properties, it was concluded that the third layer of a five-layer slab could be already considered bulklike. This was further confirmed on the basis of tests performed with a seven-layer slab. Most of the calculations were performed employing supercells with a 3 × 2 in-plane periodicity, with 1−5 Ni adatoms, corresponding to a coverage of 1/6−5/6 ML. Larger supercells were used to describe some mechanisms such as adatom surface diffusion and Ni diffusion in bulk Cu. Energy barriers were calculated using the Nudged Elastic Band method.[32] Other technical details (energy cutoff, thresholds, smearing, k-point set for Brillouin-zone sampling) are similar to those described in refs 14−17.

## ■ RESULTS AND DISCUSSION

In this work, Ni and Cu segregation and aggregation were investigated on the Cu(110) single-crystal termination. After standard sputtering and annealing cycles under UHV conditions, the Cu(110) sample was cooled down to 170 K for Ni ad-layer evaporation from a hot Ni filament. On the basis of the results reported in refs 21 and 22, at this temperature, Ni adatoms can diffuse on the Cu surface, thus forming 2D Ni ad-islands thanks to the strong Ni−Ni attractive lateral interaction, without penetrating the bulk. Mild annealing to 270 K yields surface reordering, as confirmed by a sharp (1 × 1) LEED pattern. In Figure 1a, Cu and Ni 3p X-ray photoelectron spectroscopy (XPS) spectra obtained as a function of the Ni ad-coverage are shown. Fitting of the data yields the core-level binding energy evolution (Figure 1b), indicating a shift of 200−250 meV toward lower binding energies of the Ni $3p_{3/2}$ peak at submonolayer Ni coverage regimes with respect to the bulklike situation (4−6 ML). In parallel, there is no significant shift of the Cu core level. Due to the intrinsic width of the p components, surface, bulk, and interface contributions cannot be resolved from the single experimental peak. For this reason, the reported value accounts for the overall shift of the single visible peak.

In a subsequent set of measurements, starting from a surface Ni coverage of 0.75 ML, XPS was used to monitor the time evolution of the Cu and Ni core levels in real time,[33] at selected fixed temperatures. After preparation of the Ni ad-layer, the sample temperature was suddenly raised to the selected target value, following a steplike profile; a spectroscopic "movie" of the segregation process was then obtained in real time from the intensities of the corresponding spectra. In Figure 2, the evolution of the Cu (right) and Ni (left) 3p core-level intensities is reported as a function of time for different temperature values. The observed decay behavior of the Ni signal can be ascribed to the finite inelastic mean free path ($\lambda$) of the photoemitted electrons, which upon diffusion of Ni atoms into the Cu bulk, have to cross the upper layers in their travel to the crystal surface. In parallel, the Cu signal intensity raises as the Cu concentration at the surface increases.

From the above considerations, it follows that the Ni and Cu signal intensities are related to the composition profile of the sample in the direction perpendicular to the surface. In order to obtain quantitative information, we can model the diffusion and

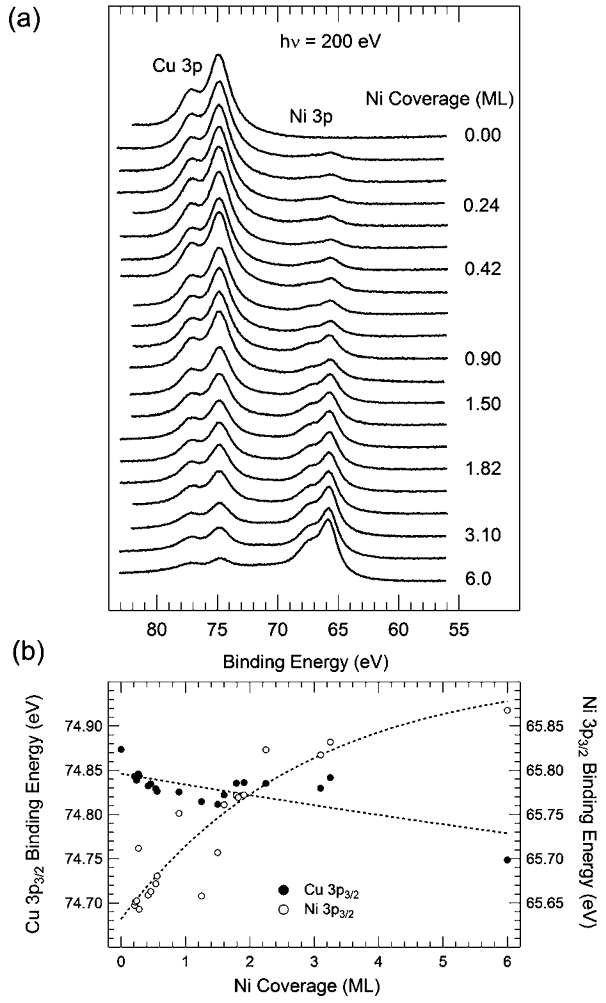

**Figure 1.** (a) Cu and Ni $3p_{3/2}$ and $3p_{1/2}$ doublets core-level spectra for increasing Ni coverage (from top to bottom). (b) Cu (left axis) and Ni (right axis) $3p_{3/2}$ core-level binding energies as a function of the Ni ad-layer coverage. Dashed lines in (b) are drawn to guide the eye.

segregation processes considering exchange mechanisms between adjacent layers, including the initial Ni ad-layer. In general, the average Ni concentration of the $n$-th layer ($\theta_{n\geq 0}$) will be determined by the flux balance of Ni atoms from and to the $(n-1)$-th and $(n+1)$-th adjacent layers. This yields an infinite system of time-dependent differential rate equations, each describing the $n$-th layer concentration evolution for Ni:

$$\frac{\partial \theta_n}{\partial t} = -\theta_n(1-\theta_{n-1})R_{n,n-1} - \theta_n(1-\theta_{n+1})R_{n,n+1} + \theta_{n-1}(1-\theta_n)R_{n-1,n} + \theta_{n+1}(1-\theta_n)R_{n+1,n} \tag{1}$$

The quantities $R_{n,m}$ are the exchange rates from the $n$-th to the $m$-th layer and are related to the prefactors ($\nu_0$), the exchange barriers ($\Delta E_{n,m}$), and the temperature by the Arrhenius law $R_{n,m} = \nu_0\exp(-\Delta E_{n,m}/k_BT)$. In general the barriers $\Delta E_{n,m}$ can depend on the concentrations $\theta_n$ and $\theta_m$ and on other configuration details (local composition, defects, steps), but in our model, we consider constant average values. We also set $\nu_0$ to a standard value of $10^{12}$ s$^{-1}$, equal for both Ni and Cu rates and consistent with reference literature.[34] We will show that close to the surface, as it might be expected, the direct and reverse diffusion rates are not equal ($R_{n,n+1} > R_{n+1,n}$), while deeper into the crystal bulk $R_{n,n\pm 1} = R_{n\pm 1,n} = R_{\text{bulk}}$ due to symmetry reasons, where $R_{\text{bulk}} = \nu_0\exp(-\Delta E_{\text{bulk}}/k_BT)$. It is interesting to note, for the sake of generality, that in the latter case the model equations describing the process converge to

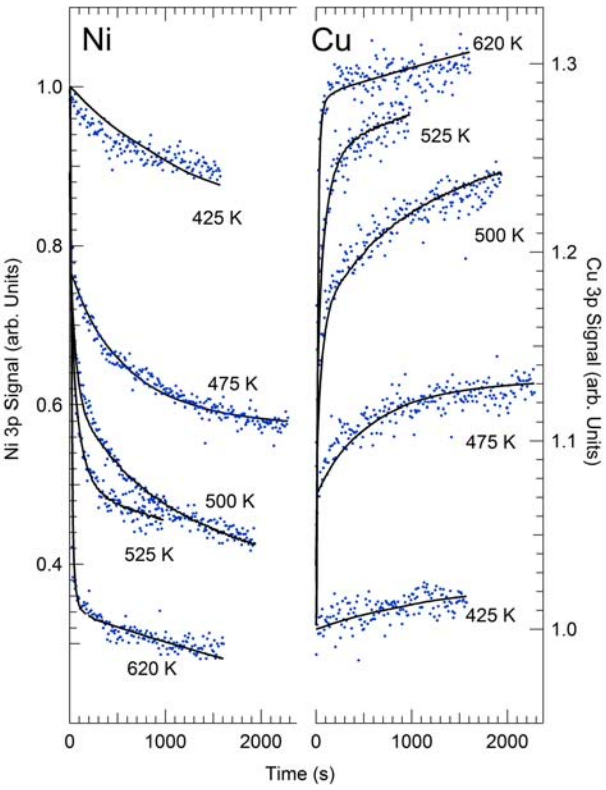

**Figure 2.** Time evolution of the normalized Ni and Cu 3p core-level intensities at selected, fixed temperatures after Ni deposition at 170 K. Initial Ni coverage: 0.75 ML. Photon energy: 200 eV. Both experimental data (dots) and best fit modeling (lines) are shown.

$$\frac{\partial \theta_n}{\partial t} = [\theta_{n+1} - 2\theta_n + \theta_{n-1}]R_{\text{bulk}} \tag{2}$$

which is indeed the discretized form of the Fick's second law of diffusion

$$\frac{\partial \theta}{\partial t} = D\frac{\partial^2 \theta}{\partial x^2} \tag{3}$$

with $R_{\text{bulk}} = D/2$. In our case $n = 0$ refers to the ad-layer, and $\theta_0(0)$ coincides with the initial Ni coverage in ML. $R_{-1,0}$ and $R_{0,-1}$ are set to zero, since during the experiment, no Ni deposition nor evaporation occurred. In the present case, the initial condition is $\theta_0(0) = 0.75$ ML and $\theta_{n>0}(0) = 0$ ML. The experimental signal $S_{\text{Ni}}(t)$ extracted from the Ni $3p_{3/2}$ peak area was normalized ($S_{\text{Ni}}(0) = 1$) and can be expressed as follows:

$$S_{\text{Ni}}(t) = \frac{1}{\theta_0(0)}\{\theta_0(t) + \sum_{n>0}\theta_n(t)[(1-\theta_0(0))\mathrm{e}^{-(n-1)\Delta x/\lambda} + \theta_0(0)\mathrm{e}^{-n\Delta x/\lambda}]\} \tag{4}$$

while for Cu we can write

$$S_{\text{Cu}}(t) = 1 + \alpha(1 - S_{\text{Ni}}(t)) \tag{5}$$

where the proportionality coefficient between the Ni and Cu signals ($\alpha$) accounts for the different photoionization cross section. Measurements were performed with a photon energy of 200 eV, corresponding to an average photoelectron mean free path $\lambda$ of 4.3 Å for both Cu and Ni,[35] to be compared with the Cu(110) interlayer distance $\Delta x = 1.245$ Å. Consequently, when fitting the experimental data in Figure 2, we can simplify the model and consider in detail only the time evolution of the composition of the topmost layers and of the corresponding signal. Considering the first three layers we obtain the following:

$$\frac{\partial\theta_0}{\partial t} = -\theta_0(1-\theta_1)R_{0,1} + \theta_1(1-\theta_0)R_{1,0} \tag{6}$$

$$\begin{aligned}\frac{\partial\theta_1}{\partial t} &= -\theta_1(1-\theta_0)R_{1,0} - \theta_1(1-\theta_2)R_{1,2}\\ &\quad + \theta_0(1-\theta_1)R_{0,1} + \theta_2(1-\theta_1)R_{2,1}\end{aligned} \tag{7}$$

$$\begin{aligned}\frac{\partial\theta_2}{\partial t} &= -\theta_2(1-\theta_1)R_{2,1} - \theta_2(1-\theta_3)R_{2,3}\\ &\quad + \theta_1(1-\theta_2)R_{1,2} + \theta_3(1-\theta_2)R_{3,2}\end{aligned} \tag{8}$$

$$\begin{aligned}\frac{\partial\theta_3}{\partial t} &= -\theta_3(1-\theta_2)R_{3,2} - \theta_3(1-\theta_4)R_{3,4}\\ &\quad + \theta_2(1-\theta_3)R_{2,3} + \theta_4(1-\theta_3)R_{4,3}\end{aligned} \tag{9}$$

Since the experimental information contained in the data does not allow determination of all the parameters included in these equations, further suitable approximations are needed. Considering that for deeper layers (i) the signal contribution is exponentially weaker and (ii) the exchange rates are expected to be lower (i.e., $\Delta E_{n,n+1}$ grows with $n$), we assume $R_{3,2} = R_{3,4} = R_{4,3} = 0$. This assumption implies that only the signal from the first three layers is considered. Accordingly, eq 9 simplifies into $\partial\theta_3/\partial t\ \theta_2(1-\theta_3)R_{2,3}$ yielding convergence of the least-squares fitting procedure. For layers deeper than the third, the diffusion of Ni atoms into a bulk reservoir can be accounted for by the following equation:

$$S_{\mathrm{Ni},n>3}(t+dt) = S_{\mathrm{Ni},n>3}(t)\mathrm{e}^{-R_{\mathrm{bulk}}dt\Delta x/\lambda} \tag{10}$$

The curves in Figure 2 were fitted with the above model, allowing the simultaneous determination of seven free parameters: $\Delta E_{0,1}$, $\Delta E_{1,0}$, $\Delta E_{1,2}$, $\Delta E_{2,1}$, $\Delta E_{2,3}$, $\Delta E_{\mathrm{bulk}}$, and $\alpha$. In the data fitting procedure, we also considered the transient contribution in the steplike surface annealing to the selected target temperature; that is, we used the experimentally determined $T(t)$ function. From Figure 2, it can be observed that the experimental data (dots) are well reproduced by the simplified modeling adopted (lines). The corresponding quantitative values of the fitting parameters are summarized in the Experiment column of Table 1, showing a trend where $\Delta E_{n,n+1}$ grows with $n$ and $\Delta E_{n,n+1} < \Delta E_{n+1,n}$, therefore justifying the assumptions of our model.

As already mentioned, the barriers $\Delta E_{n,m}$ can depend not only on the average concentrations $\theta_n$ and $\theta_m$ but also on the local environment and specific site-exchange mechanisms. The experimentally measured quantities are indeed an average over several possible parallel and competing mechanisms. In order to shed light on the role of the local environment on the measured quantities, we used an ab initio approach. Local Ni coverage, defects, and different involved mechanisms (hopping, exchange, etc) were considered in order to identify the most favored processes and to define an energy range for the barriers of the main rate-limiting steps, depending on the very local geometry. In this search, a large set of DFT calculations was performed in (3 × 2) and (4 × 2) unit cells for different Ni ad-layer coverage values, ranging from 1/6 to 5/6 ML. The exchange barriers for a single Ni atom (obtained for a starting configuration with Ni only in the ad-layer and with no defects) are summarized in the two Theory columns of Table 1, depending on the coverage. The experimentally observed trend is confirmed in both cases, yielding values for $\Delta E_{n,n+1}$ growing with $n$ and in most cases $\Delta E_{n,n+1} < \Delta E_{n+1,n}$. Larger ranges (not reported here) are obtained when including other starting configurations (for instance with Ni occupying both ad-layer and surface sites). DFT barriers for surface diffusion via hopping and exchange mechanisms are reported in Table 2. We want to stress that barriers reported in Table 1 are related to Ni diffusion in the direction perpendicular to the surface, while Table 2 refers to diffusion at the surface.

**Table 1. Experimental and Calculated (DFT) Barriers for Ni−Cu Exchange between Layers and in the Bulk**[a]

| | experiment | theory | |
|---|---|---|---|
| | 0.75 ML | 0.17 ML | 0.83 ML |
| $\Delta E_{0,1}$ | 1.20 ± 0.15 | 0.17 | 0.86 |
| $\Delta E_{1,0}$ | 1.25 ± 0.15 | 0.48 | 1.23 |
| $\Delta E_{1,2}$ | 1.40 ± 0.05 | 0.91 | 1.70−2.22 |
| $\Delta E_{2,1}$ | 1.50 ± 0.20 | 1.22 | 0.89−2.70 |
| $\Delta E_{2,3}$ | 1.60 ± 0.15 | 2.19 | |
| $\Delta E_{\mathrm{bulk}}$ | 2.00 ± 0.20, 2.32[b] | 0.78[c]−4.0 | |

[a] All values are in eV. DFT energy ranges are reported when different possible paths have been considered. [b] Experimental value for Ni diffusion in a bulk Cu crystal;[37] literature reference values for bulk self-diffusion barriers are 2.05 eV (Cu in Cu) and 2.9 eV (Ni in Ni).[38] [c] When a vacancy is present, the bulk exchange barrier is much lower.

**Table 2. DFT Energy Barriers for Surface Diffusion and Adatom/Surface-Atom Exchange Mechanisms along the Main Surface Directions (Ad-Layer Coverage 1/6 ML)**[a]

| adatom/ host | diffusion $[1\bar{1}0]$ | diffusion [001] | exchange |
|---|---|---|---|
| Cu/Cu | 0.23 (0.08−0.76) | 1.15 (1.31−1.32) | 0.29 (0.09−0.63) |
| Ni/Ni | 0.27 (0.18−0.96) | 2.14 (1.68) | 0.53 (0.25−1.02) |
| Ni/Cu | 0.17 | 0.48[b]−1.60 | 0.17 |

[a] All values are in eV. Hopping is the standard mechanism for surface diffusion, but also the exchange mechanism may drive adatoms along both crystallographic directions. Values in parentheses represent reference ranges from data in the literature.[39−44] [b] Diffusion occurs via a Ni−Cu/Cu−Ni exchange process involving two Cu and one Ni atoms.

In Figure 3, we represent the energy diagram for the diffusion/segregation mechanisms of a single Ni atom that show the smallest activation barriers among several investigated paths. The upper panel (a) presents the paths for a Ni adatom starting from a low-coverage configuration (0.17 ML), while the lower panel (b) refers to a starting configuration of 0.83 ML. Competing elementary processes leading to aggregation or segregation are compared. Close inspection of the processes shown in the figure leads to the following conclusions: (i) in all cases, there is an energy gain when Ni penetrates the Cu bulk progressively from layer 0 to 1 and 2, whereas no further gain is obtained in going to deeper layers; (ii) for deep layers, the energy barriers that have to be overcome are high with respect to the system temperature, thus indicating the relevance of kinetic limits to the processes; (iii) these barriers vary

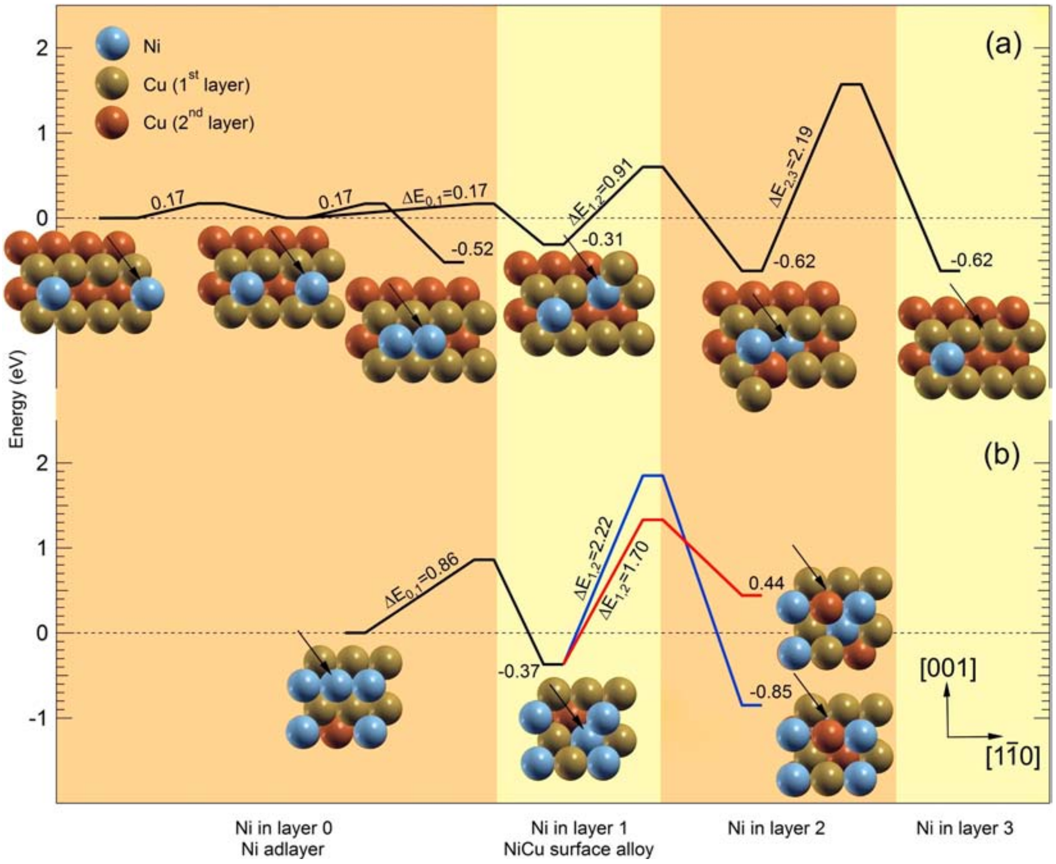

**Figure 3.** Results obtained by means of DFT calculations of selected diffusion/segregation paths for a single Ni atom starting from Ni only in the ad-layer. (a) Ni ad-dimer formation/disaggregation and Ni adatom diffusion/segregation (low coverage, corresponding to Table 1, column 2); (b) 5/6 ML (corresponding to Table 1, column 3): the two colored paths differ due to the formation of a Cu vacancy in the second layer (blue path). Black arrows indicate the position of the segregating/diffusing Ni atom.

significantly by changing the Ni concentration (panel a with respect to b), while the energies of the final configurations remain comparable. This is a key point, showing that the segregation behavior, determined by kinetics and ultimately by the Ni–Ni interaction, can be directly controlled by finely tuning of the Ni coverage.

From the set of possible processes that were investigated, a picture can be obtained for the Ni–Cu system, which is detailed in the following. A single Ni adatom binds to the Cu(110) surface with an energy of 4.31 eV (DFT value), larger than that for a Cu adatom (3.65 eV). Its penetration barrier into the Cu first layer ($\Delta E_{0,1}$ in Table 1 and Figure 3a), the surface diffusion barrier along the troughs in the [1$\bar{1}$0] direction (Table 2), and the aggregation barrier are all equal to 0.17 eV (Figure 3a), thus indicating competing mechanisms. The strong Ni–Ni attractive interaction (0.48–0.52 eV per Ni–Ni bond in the ad-layer depending on the local coverage) favors the latter mechanism, thus promoting the nucleation of 2D islands when Ni is evaporated at low substrate temperature and preventing island disaggregation and dissolution of Ni adatoms into the Cu bulk (Figure 3b), as confirmed experimentally by our data (the XPS signal remains constant up to room temperature) in agreement with previous reports.[21,22] For the surface diffusion of a Ni adatom along the [001] direction, instead, higher energy barriers were found (Table 2); hopping between troughs via the short bridge Cu sites is limited by a high barrier (1.60 eV) whereas a barrier of only 0.48 eV was found when considering an alternative route involving multiple exchange processes with the substrate, where the Ni adatom replaces a Cu atom in the first layer and then it pops up again in the adjacent trough, being substituted by a diffusing Cu adatom. The nonisotropic diffusion explains previously observed formation of Ni islands that are elongated in the [1$\bar{1}$0] direction.[25] Scanning tunneling microscopy imaging revealed the presence of rectangular-shaped ad-islands in the submonolayer regime. Aggregation of Ni or Cu into ad-islands is further favored by a Ni atom already embedded in the Cu surface below the island (additional 0.20 and 0.10 eV energy gain, respectively), thus identifying a single Ni atom embedded in the first layer as a potential ad-island nucleation center. At temperatures higher than room temperature (RT), more energy is available, and additional processes become accessible. Ni ad-island disaggregation and stabilization of a surface NiCu alloy layer occur with barriers in the 0.65–1.0 eV range. By overcoming a barrier of 0.91 eV ($\Delta E_{1,2}$ in Figure 3a), a first layer (surface) embedded Ni atom can diffuse to the second layer and progressively into the bulk ($\Delta E_{2,3}$ = 2.19 eV). For the latter steps, barriers up to 4 eV have been obtained for Ni–Cu exchange in a perfect bulk crystal (highest value of $\Delta E_{\mathrm{bulk}}$ in Table 1). However, when introducing defects, vacancies, and cooperative mechanism, assisted diffusion occurs in the bulk with barriers as low as 0.78 eV (lowest value of $\Delta E_{\mathrm{bulk}}$ in Table 1). The measured value (2.0 eV) is within the range.

In order to further validate our segregation model, which has been used to fit the experimental spectroscopic data in light of the theoretical considerations, we performed a second experiment, in which the Ni 3p core-level signal was collected for different initial Ni coverage values (2.25, 0.9, and 0.3 ML) while the sample temperature, after Ni deposition at low $T$, was linearly increased in a temperature programmed (TP) experiment.[36] The temperature derivative of the Ni signal (proportional to the rate) at $\theta_{\mathrm{Ni}}$ = 2.25 ML is reported in Figure 4a in order to highlight the rate-limiting steps, as indicated by the vertical shaded areas and by the corresponding text labels. The latter were assigned on the basis of the novel results obtained by our modeling, except from the interface alloy phase that was already investigated in a previous theoretical study.[23] In Figure 4b, the XPS Ni signal intensity is reported as a function of temperature (dots). The heating rate was 0.1 K/s. The continuous lines are obtained by integrating the model differential equations with the experimental barriers (Table 1) obtained from data in Figure 2 and using the $T(t)$ function from the new experiment, thus with no fitting to the data. In practice, data from the time-decay experiment were used to successfully describe the system behavior observed in the TP experiment. The agreement is remarkable, in light of the simplicity of the model and despite that different Ni coverage values are involved in the experiments, thus providing an independent proof that our approach properly captures the main involved rate-limiting processes. The detailed Ni coverage evolution for the ad-layer and the first three crystal layers, as obtained from the model, is reported in Figure 4c for both the 0.9 and 0.3 ML experiments. The 2.25 ML experiment deserves an additional discussion. In the multilayer case, indeed, a new reaction step was observed, as confirmed by the LEED patterns. When heating, an interface NiCu alloy is initially formed under the Ni film, accordingly to literature.[23] Second, a surface reconstruction occurs in which faceting is observed (see the Supporting Information).

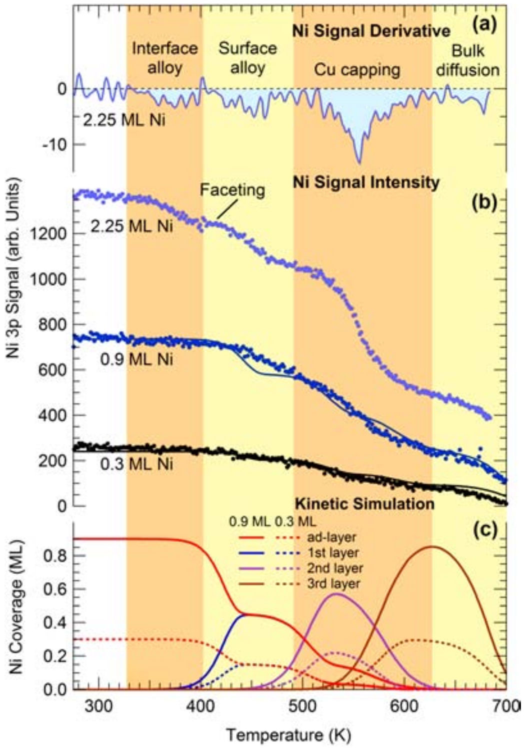

**Figure 4.** Temperature programmed photoelectron spectroscopy measurement of the Ni 3p core level. (a) The temperature derivative of the XPS signal intensity provides evidence for the presence of concatenated, distinct steps involved in the process, indicated by the vertical yellow and orange shaded areas; (b) experimental signal intensities (dots) are compared with the results from modeling of the segregation/diffusion processes (lines); (c) detailed evolution of the single-layer Ni concentration as obtained from the modeling for the 0.3 ML (dashed lines) and 0.9 ML (continuous lines) cases.

## CONCLUSIONS

Thanks to the combination of in situ time-resolved experiments with DFT calculations, we have provided new insight in the mechanisms at the basis of the interplay between energetic and kinetic effects in the Ni–Cu diffusion and segregation processes. The latter define the actual alloy surface properties, which is exploited for several relevant applications. From the novel information about the rate-limiting steps and segregation/diffusion/aggregation channels, we show that Ni–Ni interaction plays an important role in the Ni–Cu exchange process, which is at the basis of Ni migration into the bulk and segregation to the surface. We actually demonstrate and confirm the validity of the tentative hypothesis elaborated in ref 23 where the authors postulated an important role of kinetics. Indeed, we show that the Ni segregation barriers are strongly influenced by the local Ni concentration. By providing a couple of selected examples, our results are relevant in understanding graphene growth[9,10] and in determining catalytic activity. Additionally, the chemical potential and the interaction of adsorbed reactants and reaction products with the surface can influence the Ni surface concentration and the actual surface alloy composition. As in the case of the $H_2$–CO–$CO_2$/Ni/Cu reaction,[13,20] one of the possible methods in order to tune the catalyst activity by governing the Ni surface coverage is to properly define the concentration ratios of both reactants and spectator species. The latter do not take part in the reaction but influence the Ni/Cu segregation process and consequently the catalyst activity. This effect is demonstrated to be crucial also under standard reaction conditions,[13] where it was observed in the case of the $CO_2$ reduction reaction on a Ni/Cu model catalyst. In conclusion, a detailed knowledge of the nanokinetic mechanisms governing the atomic segregation and self-diffusion in bimetallic alloys allows active control of specific surface properties of great scientific and technological relevance.

## ASSOCIATED CONTENT

### Ⓢ Supporting Information

Images of the LEED patterns and a discussion of the reconstruction. This material is available free of charge via the Internet at http://pubs.acs.org.

## AUTHOR INFORMATION

### Corresponding Author

vesselli@iom.cnr.it

### Present Address

◆International School for Advanced Studies (SISSA), via Bonomea 265, I-34136 Trieste, Italy.

### Notes

The authors declare no competing financial interest.

## ■ ACKNOWLEDGMENTS

E.V., M.P., and A.B. acknowledge financial support from MIUR through Futuro in Ricerca FIRB 2010 project no. RBFR10J4H7. Financial support from MIUR through the PRIN 2008 project no. 20084E2WFX is also acknowledged. C.A. and C.D. acknowledge support from CNR through the ESF FANAS project NOMCIS. Computational resources have been partly obtained through Italian SuperComputing Resource Allocation (ISCRA) grants of the Consorzio Interuniversitario CINECA, partly within the agreement between the University of Trieste and CINECA. We thank A. Locatelli for helpful discussions. We are grateful to S. Lizzit and A. Baraldi for their contribution.

## ■ REFERENCES

(1) Chellali, M. R.; Balogh, Z.; Bouchikhaoui, H.; Schlesiger, R.; Stender, P.; Zheng, L.; Schmitz, G. *Nano Lett.* **2012**, *12*, 3448.
(2) Vesselli, E.; Baraldi, A.; Lizzit, S.; Comelli, G. *Phys. Rev. Lett.* **2010**, *105*, 046102.
(3) Stierle, A.; Renner, F.; Streitel, R.; Dosch, H.; Drube, W.; Cowie, B. C. *Science* **2004**, *303*, 1652.
(4) Kresse, G.; Schmid, M.; Napetsching, E.; Shishkin, M.; Köler, L.; Varga, P. *Science* **2005**, *308*, 1440.
(5) Baraldi, A.; Giacomello, D.; Rumiz, L.; Moretuzzo, M.; Lizzit, S.; Buatier De Mongeot, F.; Paolucci, G.; Comelli, G.; Rosei, R.; Nieuwenhuys, B. E.; Valbusa, U.; Kiskinova, M. P. *J. Am. Chem. Soc.* **2005**, *127*, 5671.
(6) Taylor, K. C. *Automobile Catalytic Converters*; Springer-Verlag: Berlin, Germany, 1984.
(7) Kokubo, T.; Kim, H.-M.; Kawashita, M. *Biomaterials* **2003**, *24*, 2161.
(8) Piscanec, S.; Colombi Chiacchi, L.; Vesselli, E.; Comelli, G.; Sbaizero, O.; Meriani, S.; De Vita, A. *Acta Mater.* **2004**, *52*, 1237.
(9) Li, X.; Cai, W.; Colombo, L.; Ruoff, R. S. *Nano Lett.* **2009**, *9*, 4268.
(10) Liu, X.; Fu, L.; Liu, N.; Gao, T.; Zhang, Y.; Liao, L.; Liu, A. *J. Phys. Chem. C* **2011**, *115*, 11976.
(11) Chen, S.; Brown, L.; Levendorf, M.; Cai, M.; Ju, S.; Edgeworth, J.; Li, X.; Magnuson, C. W.; Velamakanni, A.; Piner, R. D.; Kang, J.; Park, J.; Ruoff, R. S. *ACS Nano* **2011**, *5*, 1321.
(12) Ernst, A.; Lueders, M.; Temmerman, W. M.; Szotek, Z.; van der Laan, G. *J. Phys.: Condens. Matter* **2000**, *12*, 5599.
(13) Nerlov, J.; Chorkendorff, I. *J. Catal.* **1999**, *181*, 271.
(14) Ding, X.; De Rogatis, L.; Vesselli, E.; Baraldi, A.; Comelli, G.; Rosei, R.; Savio, L.; Vattuone, L.; Rocca, M.; Fornasiero, P.; Ancilotto, F.; Baldereschi, A.; Peressi, M. *Phys. Rev. B* **2007**, *76*, 195425.
(15) Vesselli, E.; De Rogatis, L.; Ding, X.; Baraldi, A.; Savio, L.; Vattuone, L.; Rocca, M.; Fornasiero, P.; Peressi, M.; Baldereschi, A.; Rosei, R.; Comelli, G. *J. Am. Chem. Soc.* **2008**, *130*, 11417.
(16) Vesselli, E.; Rizzi, M.; De Rogatis, L.; Ding, X.; Baraldi, A.; Comelli, G.; Savio, L.; Vattuone, L.; Rocca, M.; Fornasiero, P.; Baldereschi, A.; Peressi, M. *Phys. Chem. Lett.* **2010**, *1*, 402.
(17) Dri, C.; Peronio, A.; Vesselli, E.; Africh, C.; Rizzi, M.; Baldereschi, A.; Peressi, M.; Comelli, G. *Phys. Rev. B* **2010**, *82*, 165403.
(18) Vesselli, E.; Schweicher, J.; Bundhoo, A.; Frennet, A.; Kruse, N. *J. Phys. Chem. C* **2011**, *115*, 1255.
(19) Yang, Y.; White, M. G.; Liu, P. *J. Phys. Chem. C* **2012**, *116*, 248.
(20) Nerlov, J.; Chorkendorff, I. *Catal. Lett.* **1998**, *54*, 171.
(21) Demirci, E.; Winkler, A. *Surf. Sci.* **2010**, *604*, 609.
(22) Demirci, E.; Carbogno, C.; Groß, A.; Winkler, A. *Phys. Rev. B* **2009**, *80*, 085421.
(23) Meyerheim, H. L.; Sander, D.; Negulyaev, N. N.; Stepanyuk, V. S.; Popescu, R.; Popa, I.; Kirschner, J. *Phys. Rev. Lett.* **2008**, *100*, 146101.
(24) Tzeng, Y. R.; Wu, H.; Shiang, K.-D.; Tsong, T. T. *Phys. Rev. B* **1993**, *48*, 5549.
(25) Nünthel, R.; Lindner, J.; Poupoulos, P.; Baberschke, K. *Surf. Sci.* **2004**, *566–568*, 101.
(26) Domnick, R.; Held, G.; Koschel, H.; Ammon, Ch.; Steinrück, H.-P. *Surf. Sci.* **2001**, *482–485*, 1292.
(27) Pourovskii, L. V.; Skorodumova, N. V.; Vekilov, Yu. Kh.; Johansson, B.; Abrikosov, I. A. *Surf. Sci.* **1999**, *439*, 111.
(28) Doniach, S.; Sunjic, M. *J. Phys. C: Solid State Phys.* **1970**, *3*, 285.
(29) Perdew, J. P.; Burke, K.; Ernzerhof, M. *Phys. Rev. Lett.* **1996**, *77*, 3865.
(30) Giannozzi, P.; Baroni, S.; Bonini, M.; Calandra, M.; Car, R.; Cavazzoni, C.; Ceresoli, D.; Chiarotti, G. L.; Cococcioni, M.; Dabo, I.; Dal Corso, A.; de Gironcoli, S.; Fabris, S.; Fratesi, G.; Gebauer, R.; Gerstmann, U.; Gougoussis, C.; Kokalj, A.; Lazzeri, M.; Martin-Samos, L.; Marzari, N.; Mauri, F.; Mazzarello, R.; Paolini, S.; Pasquarello, A.; Paulatto, L.; Sbraccia, C.; Scandolo, S.; Sclauzero, G.; Seitsonen, A. P.; Smogunov, A.; Umari, P.; Wentzcovitch, R. M. *J. Phys.: Condens. Matter* **2009**, *21*, 395502.
(31) Ultrasoft pseudopotentials from the publicly available QUANTUM ESPRESSO table are used.
(32) Jónsson, H.; Mills, G.; Jacobsen, K. W. *Classical and Quantum Dynamics in Condensed Phase Simulations*; World Scientific: Singapore, 1998; pp 385–404.
(33) Baraldi, A.; Comelli, G.; Lizzit, S.; Kiskinova, M.; Paolucci, G. *Surf. Sci. Rep.* **2003**, *49*, 169.
(34) Kong, L. T.; Lewis, L. J. *Phys. Rev. B* **2006**, *74*, 073412.
(35) Tanuma, S.; Powell, C. J.; Penn, D. R. *Surf. Interface Anal.* **2003**, *35*, 268.
(36) Baraldi, A.; Comelli, G.; Lizzit, S.; Cocco, D.; Paolucci, G.; Rosei, R. *Surf. Sci.* **1996**, *367*, L67.
(37) Almazouzi, A.; Macht, M.-P.; Naundorf, V.; Neumann, G. *Phys. Rev. B* **1996**, *54*, 587.
(38) Jackson, K. A. *Kinetic Processes: Crystal Growth, Diffusion, and Phase Transitions in Materials*; Wiley-VCH Verlag GmbH & Co.: Weinheim, Germany, 2004; p 29.
(39) Agrawal, P. M.; Rice, B. M.; Thompson, D. L. *Surf. Sci.* **2012**, *515*, 21.
(40) Liu, C. L.; Cohen, J. M.; Adams, J. B.; Voter, A. F. *Surf. Sci.* **1991**, *253*, 334.
(41) Tung, R. T.; Graham, W. R. *Surf. Sci.* **1980**, *97*, 73.
(42) Wen, Y.-N.; Zhang, J.-M.; Xu, K.-W. *Appl. Surf. Sci.* **2009**, *256*, 1521.
(43) Montalenti, F.; Ferrando, R. *Phys. Rev. B* **1999**, *59*, 5881.
(44) Perkins, L. S.; DePristo, A. E. *Surf. Sci.* **1994**, *317*, L1152.